Orientation-dependent ionization rate of diatomic molecules

Paul Winter and Manfred Lein[*]

Institute of Theoretical Physics, Leibniz University Hannover, Appelstraße 2, 30167 Hannover, Germany

The ionization rate of molecules in strong laser fields depends on the orientation of the ionizing electric field relative to the molecular frame. The orientation dependence of the rate plays an important role in strong-field-based attosecond-scale and imaging methods, motivating us to investigate theoretically whether it can be extracted from the ionization yields or photoelectron momentum distributions obtained by ionization with laser pulses of various polarization forms. As a reference for comparison we use the orientation dependence of the static-field tunneling rate. Numerical solutions of the time-dependent Schrödinger equation for ionization of the ground and first excited states of a model HeH^+ molecule show that linearly or circularly polarized single-color pulses are of limited use for obtaining the orientation-dependent rate accurately. By adding a second harmonic with suitable polarization, i.e., using either linearly polarized two-color fields or counterrotating circularly polarized two-color fields, the agreement of the extracted signal with the exact tunneling rate is substantially improved.

I. INTRODUCTION

In strong-field ionization, the probability that one bound electron leaves an atom or molecule due to the presence of an external laser pulse is known as the single-electron ionization yield. Viewing this type of ionization as a time-dependent process, the yield is an accumulated signal incorporating the ionization amplitudes at all possible times. Furthermore, since for low frequencies the instantaneous ionization rate is generally proportional to an exponential factor $\exp[-2(2I_p)^{3/2}/(3E)]$ with the instantaneous electric field E and the ionization potential I_p in the exponent [1], ionization is dominated by the largest electric field occurring during the pulse. The ionization rate is a crucial factor in strong-field phenomena such as high-harmonic generation [2], laser-induced electron diffraction (LIED) [3–7], and photoelectron holography [8–10]. Therefore, accurate knowledge of ionization rates is needed to improve models for strong-field techniques such as LIED. Numerous studies have aimed at calculating the ionization yield in accordance with experiments [11–29]. Reproducing experimental results helps to verify assumptions and validate theoretical models. However, it is uncertain whether such results can be directly applied to other contexts, such as LIED, since they might be influenced more by the specific field polarization than by the intrinsic properties of the target. While the exponential behavior of the ionization rate is well known, the prefactor, depending on the

orbital structure of the target system, needs more complicated theory [30–32]. With the ability to control the orientation of molecules in strong-field experiments with alignment pulses [5,12,16,21,26,33,34] or to obtain the orientation of the molecule after ionization using coincidence measurements of the freed electron and the residual ions [13,14,35], the ionization behavior of molecules has gained increasing interest, in particular concerning the dependence on the molecular orientation. Although atomic theories, such as the strong-field approximation or the weak-field asymptotic theory, can be extended to molecules [19,36–40], solving the time-dependent Schrödinger equation (TDSE) is still considered the most accurate approach for obtaining ionization yields for a given system [19,41]. There are several known aspects influencing the orientation-dependent ionization yield. Generally, the structure and especially the symmetry of the highest occupied molecular orbital qualitatively determine the orientation dependence [16,18,23,25,42]. However, also the possible ionization of lower-lying orbitals [14,20,22,43], a Stark-shifted ionization potential [15,24], or multielectron effects [27,44,45] can play a role. Most of these studies have used either single-color circularly or linearly polarized laser pulses with limited discussion of the question whether the target-specific properties might be masked by dependences on the polarization of the ionizing field. On the one hand, linearly polarized fields seem appropriate because they have a well-defined relative orientation between the molecular frame and the electric-field vector. For asymmetric molecules, however, two opposite field directions will usually contribute to ionization within the same pulse and thus mix electrons originating from opposite sides of the molecule [23,29]. Rescattering can further influence the ionization process in linearly polarized fields [46]. Therefore, the knowledge of the orientation-dependent total ionization yield in linear polarization is of limited use for modeling the instantaneous ionization

---

[*]Contact author: lein@itp.uni-hannover.de

rate. On the other hand, as explained in [14,21], circularly polarized fields can ionize the molecule in all orientations in one pulse and provide a mapping of the ionization direction to the final electron momentum. The orientation-dependent rate can then be extracted from the photoelectron angular distribution. However, nonadiabatic dynamics might cause substantial differences compared to the ionization rates in linearly polarized fields, especially when the electric field points along or moves across a nodal plane of the orbital [47]. A possible interpretation is that, although ionization is suppressed when the field points along a nodal plane, the ionization rate is considerably smeared out as the electric field rotates. Shifts in the photoelectron momentum distribution due to Coulomb effects on the outgoing electrons, known as attoclock shifts [48–50], lead to additional challenges in the analysis for circular polarization.

One possible alternative to single-color linearly or circularly polarized fields is two-color fields. In linear polarization, the second color introduces an asymmetry in the electric field along the polarization direction, allowing the observation of directional dependences in asymmetric molecules [18,28,29,51]. In particular, in [28] a linearly polarized two-color pulse was used to measure the orientation dependence of the ionization process in NO molecules. A recent theoretical study [29] used time-dependent density-functional theory to obtain orientation-dependent ionization rates with single- and two-color linearly polarized pulses. Both studies compared their results with approximate models incorporating the time-dependent field, so it is still unclear to what extent the extracted rates depend on the pulse polarization.

In this article we compare the orientation-dependent ionization yield obtained with different field polarizations to the exact orientation-dependent tunneling rate, where the latter is defined as the ionization rate for a constant electric field. We observe that there are laser parameters for which neither a linearly nor a circularly polarized single-color pulse provides good agreement with the exact tunneling rate, even when chosen such that the Keldysh parameter $\gamma = \omega/\omega_T$ is small ($\gamma < 1$). Here ω represents the laser frequency, while $\omega_T = E_{\text{peak}}/\sqrt{2I_p}$ is a characteristic frequency associated with instantaneous tunneling [52]. Choosing a small Keldysh parameter places the interaction in the tunneling regime. In addition to the above-mentioned fields, we investigate a two-color circularly polarized (bicircular) field that exhibits quasilinear polarization near the peak field strength [53–55]. In contrast to other studies [56–60] with bicircular fields, the used intensity ratio between both colors avoids rescattering. Both types of two-color fields offer a well-defined relative angle between the molecular axis and the direction of maximal field strength. Our analysis indicates that these two-color fields are better suited for measuring the orientation-dependent ionization rate. While in previous studies on bicircular fields [55,61] an effective frequency $\omega_{\text{eff}} > \omega$ was used in the definition of the Keldysh parameter, we use the fundamental frequency in the present work, as the effective frequency is not universally applicable to all polarizations. We focus on the HeH$^+$ molecular ion, which serves as a prototypical example of a heteronuclear diatomic molecule.
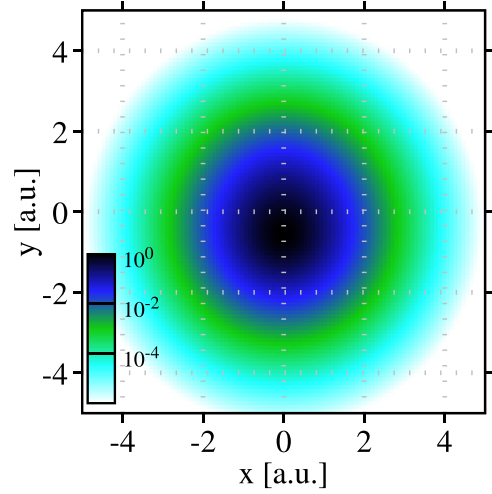

FIG. 1. Electron density $|\Psi|^2$ of the ground state of the HeH$^+$ model oriented along the y axis [$\vec{R} \parallel \hat{y}$, H at $\vec{r}_1 = (0, 0.7)^T$ a.u. and He at $\vec{r}_2 = -\vec{r}_1$].

II. NUMERICAL MODEL

We solve the TDSE for one active electron on a two-dimensional grid in dipole approximation with fixed nuclei. The sizes of the computational boxes range from 600 to 4000 a.u., with a resolution of 2048–8196 grid points in each dimension. The HeH$^+$ molecule (H at $\vec{r}_1$ and He at $\vec{r}_2$) is modeled by the potential

$$V(\vec{r}) = \frac{-1}{\sqrt{(\vec{r} - \vec{r}_1)^2 + \alpha_1}} + \frac{-\left(1 + e^{-\beta(\vec{r} - \vec{r}_2)^2}\right)}{\sqrt{(\vec{r} - \vec{r}_2)^2 + \alpha_2}}, \quad (1)$$

with $\beta = 1.063$ a.u., $\alpha_1 = \alpha_2 = 0.5$ a.u., and $|\vec{r}_1| = |\vec{r}_2| = 0.7$ a.u. [54,55]. The molecular axis is defined as $\vec{R} = \vec{r}_1 - \vec{r}_2$ with an internuclear distance $|\vec{R}| = 1.4$ a.u. Time propagation is performed using the split-operator method [62]. We start the simulations with the electron in either the ground state (see Fig. 1) or the first excited state (see Fig. 2). The ground state is calculated with imaginary-time propagation (ITP) [63]
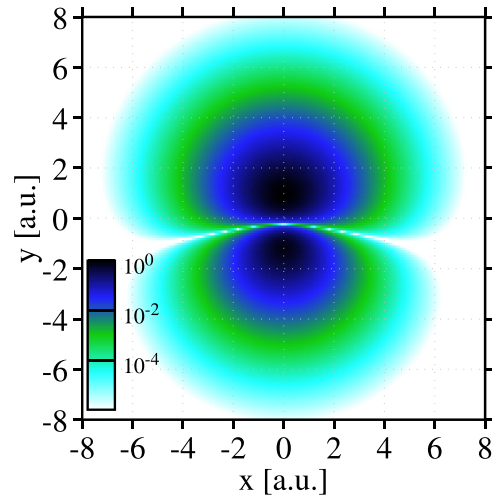

FIG. 2. Electron density $|\Psi|^2$ of the first excited state of the HeH$^+$ model oriented along the y axis [$\vec{R} \parallel \hat{y}$, H at $\vec{r}_1 = (0, 0.7)^T$ a.u. and He at $\vec{r}_2 = -\vec{r}_1$].
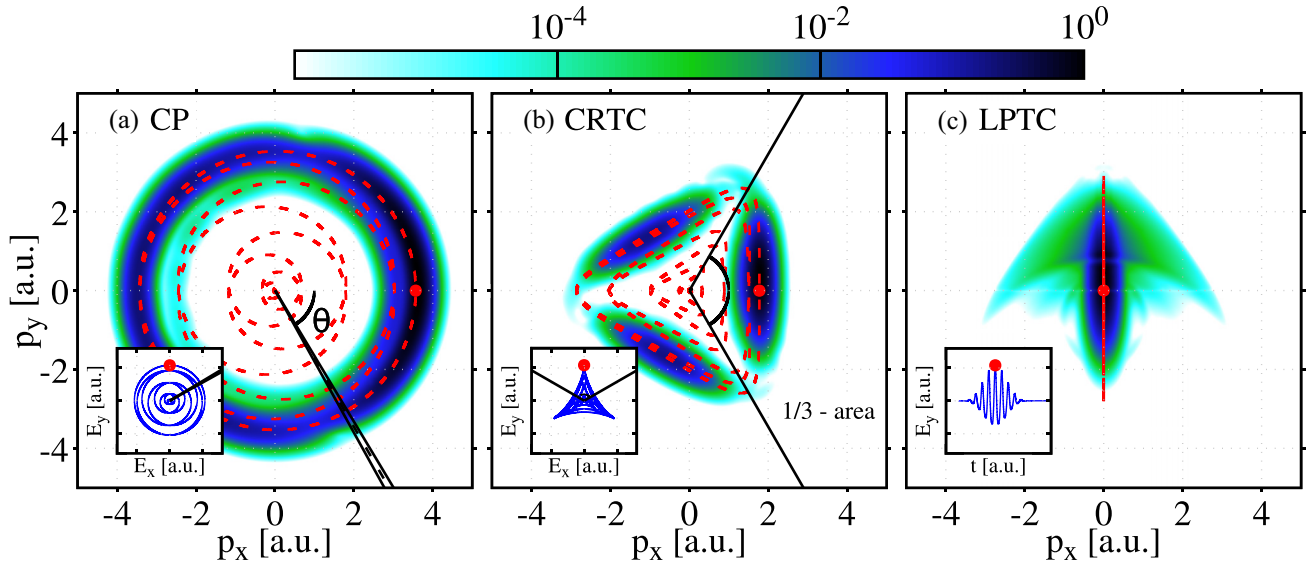
FIG. 3. Normalized photoelectron momentum distributions obtained from TDSE solutions for the first excited state of HeH$^+$ with peak electric-field strength $E_{\text{peak}} \approx 0.0542$ a.u. for different field configurations at a fundamental wavelength $\lambda = 3000$ nm: (a) the CP field, (b) the CRTC field, and (c) the LPTC field. Only for illustration, the distributions are slightly blurred by applying a Gaussian convolution filter to suppress morié patterns (see the text for details). The insets show the corresponding electrical fields $\vec{E}(t)$. The red dashed line shows the negative vector potential $-\vec{A}(t)$, red dots mark the time $t = 0$ (maximum of the electrical field), and the black solid lines indicate the integration area for the analysis. The Keldysh parameter is $\gamma = \omega \sqrt{2I_p}/E_{\text{peak}} \approx 0.36$.

and subsequent application of the real-time propagation eigenstate (RTPE) method [64]. To obtain the first excited state, we project out the ground state during the ITP and RTPE. This results in an ionization potential of $I_p \approx 1.657$ a.u. for the ground state and $I_p \approx 0.811$ a.u. for the first excited state. While we adjust the parameters of the model potential to reproduce the I_p of the HeH$^+$ ground state [54,65–68], the ionization potential of the first excited state is not related to the real molecule. This state serves as an example of a more complex orbital shape. In contrast to the ground state, the first excited state shows a nodal line in the two-dimensional electron density distribution. We expect a minimum in the orientation-dependent ionization yield at an angle where the negative electric field is approximately aligned with the nodal line. Outgoing wave packets are projected onto Volkov states using a complex absorbing potential [69]. In a small region before the absorber starts, the core potential is damped to zero.

The time-dependent vector potential is defined as

$$\vec{A}(t) = \frac{-E_{\text{peak}}}{\omega(1+\varepsilon)} f(t) \begin{pmatrix} \xi[\cos(\omega t) - \frac{\varepsilon}{2}\cos(2\omega t)] \\ \sin(\omega t) + \frac{\varepsilon}{2}\sin(2\omega t) \end{pmatrix}, \quad (2)$$

where ε is the ratio of the electric-field strength of the second harmonic to the fundamental component and ξ is an ellipticity parameter. With an envelope function $f(t)$ centered at $t = 0$, the electric field $\vec{E}(t) = -\partial_t \vec{A}(t)$ has a maximum field strength of E_{peak}. By setting ξ and ε to specific values, we can select a particular field configuration. A counterrotating two-color (CRTC) laser field [54,56–59] is achieved by $\{\xi = 1, \varepsilon \neq 0\}$. For this configuration we set ε to the ratio $\varepsilon_{\text{opt}} \approx 0.5031$, where a quasilinear polarization for an 11-cycle pulse is achieved [53–55]. An elliptically polarized

field can be constructed by setting $\varepsilon = 0$, where the special case of a circularly polarized (CP) field is realized by $\xi = 1$. In contrast, with $\xi = 0$ we select a linearly polarized two-color (LPTC) light field with ratio ε. We use $\varepsilon = 0.2$ for all calculations with LPTC fields. When both parameters ε and ξ are set to zero, a pure linearly polarized (LP) single-color field is found. Unless stated otherwise, we use the envelope function $f(t) = \cos^4(\frac{\omega t}{2N})$, with N the number of cycles.

Figure 3 shows three examples of photoelectron momentum distributions (PMDs) obtained by solving the TDSE for the first excited state of the HeH$^+$ model (see Fig. 2) oriented along the y axis. Based on the grid approach, we have a limited resolution in momentum space. Together with densely spaced above-threshold-ionization rings, this can cause an optical effect, known as moiré patterns, in the plots. We checked, by increasing the resolution, that these patterns do not influence our results. Only for illustration in Fig. 3, but not in the further analyses, we smoothed the PMDs with a Gaussian filter [70] to suppress the moiré patterns.

Figure 3(a) shows a PMD for a CP field. The inset in Fig. 3(a) shows the corresponding electrical field. The distribution follows nicely the negative vector potential (red dotted line) forming an approximate circle. The deviation from a perfect circle is caused by the envelope function and it can be reduced by increasing the duration of the pulse. In addition, the photoelectron distribution exhibits a modulation, caused by an orientation-dependent ionization rate, that remains for longer pulses. A small rotation of the distribution due to Coulomb effects, known as the attoclock angle [48–50,71], is present although difficult to notice with bare eyes. In Fig. 3(b) a PMD for a CRTC field is shown. Due to the three peaks in the electric field [see the inset in Fig. 3(b)], we also see three peaks in the PMD positioned along the negative vector

potential. The right peak, contained in the marked 1/3 area in Fig. 3(b), corresponds to ionization by the quasilinear peak when the electric field points in the $+y$ direction. While the distributions for CP pulses exhibit a small rotation, for CRTC pulses Coulomb effects cause a vertical shift (attoclock shift) of the right peak in the $+y$ direction (see [53–55]). The approximate threefold symmetry of the PMD is maintained for all molecular orientations, but the relative strengths of the peaks change. Figure 3(c) gives an example of a PMD generated by a LPTC field. This PMD is qualitatively similar to a PMD obtained with a LP pulse, but an asymmetry along the polarization direction (y direction) emerges. The inset in Fig. 3(c) shows the temporal evolution of the LPTC electric field, showing its asymmetric character.

To analyze the orientation dependence of the ionization process, we resort to two different approaches: the multishot scheme (MSS) and the single-shot scheme (SSS).

In the MSS, we repeat the TDSE simulations for varying molecular orientation but fixed field with its maximal field strength along the y axis. The orientation angle θ is then defined as the angle between the molecular axis $\vec{R} = \vec{r}_1 - \vec{r}_2$ and the y axis. We start with $\vec{R} \parallel \hat{y}$ corresponding to $\theta = 0$ [H at $\vec{r}_1 = (0, 0.7)^T = -\vec{r}_2$] and rotate the molecule counterclockwise in discrete steps. The ionization yield is obtained by integration of specific regions in the obtained PMDs. For LP and LPTC pulses, we integrate the full PMD to obtain the total ionization yield for every molecular orientation. For CRTC fields we integrate only over the main peak in the marked 1/3 area in Fig. 3(b). In this way, we select the electrons ionized by the quasilinear peak of the electric field in the y direction. In CP fields we integrate over a $2°$ angular window around the $+x$ axis. The integration is done by summation of the numerical values at the grid points inside the window. This emission direction is chosen because, based on the trajectory picture for the electron motion after departure from the parent ion, one can uniquely map the initial time of ionization to the final electron momentum. When neglecting Coulomb effects on the trajectory (simple man's model) in a CP pulse, there is a $90°$ difference between the direction of the ionizing field and the final electron emission angle. Thus, for a CP pulse with its field rotating counterclockwise in the xy plane, final momenta on the $+x$ axis correspond to ionization when the field points along the y axis.

In the SSS for CP pulses we utilize the time-momentum mapping to extract the orientation-dependent ionization rate from only one measurement, done at the molecular orientation $\vec{R} \parallel \hat{y}$. In this case, the negative polar angle in the PMD is identical to the relative angle between the molecular axis and the instantaneous electric field at the time of ionization. To obtain the orientation-dependent ionization rate, we integrate the PMD within small angular windows of $2°$. For example, the black lines in Fig. 3(a) indicate the integration area for the ionization rate at an orientation angle of $\theta = 60°$ corresponding to an electric field pointing in the direction of a polar angle of $30°$ [see the inset in Fig. 3(a)]. The SSS is not directly applicable to LP, LPTC, or CRTC pulses.

To compare the above-described approaches using finite pulses to a common reference, we calculate ionization rates by solving the TDSE for a constant electric field. After a smooth turn on, the field strength is identical to E_{peak}. We
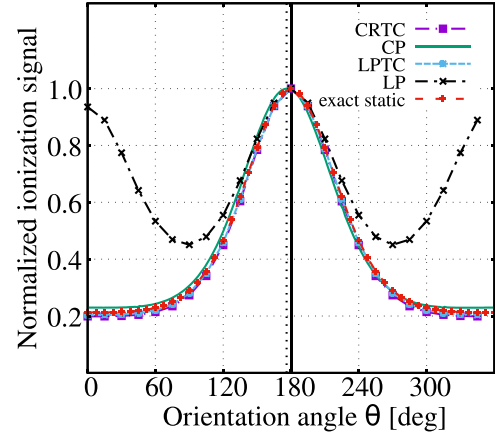

FIG. 4. Normalized ionization signal obtained from TDSE solutions starting from ground-state HeH$^+$ for different field configurations (LP, LPTC, and CRTC in the MSS and CP in the SSS) compared to the exact tunneling rate. All fields have a fundamental wavelength of $\lambda = 1200$ nm, 11 cycles, and peak electric-field strength $E_{\text{peak}} \approx 0.2033$ a.u. The dotted vertical line marks the attoclock angle of the CP pulse.

obtain an approximately steady state, which slowly decays. We fit the time-dependent squared norm to a decaying exponential function $\|\Psi(t)\|^2 \propto e^{-\Gamma t}$ to obtain the numerically exact tunneling rate Γ of the system. This procedure is carried out for different molecular orientations θ and serves as an idealized reference not available in experiments. In the following, we refer to these results as exact static, because they represent the adiabatic limit for long wavelengths eliminating the influence of frequency and polarization revealing the orientation-dependent ionization rate as a property of the molecule.

All results shown refer to sharp molecular orientation. We note that any comparison to experiments using prealignment techniques needs to take into account the experimental distribution of orientation angles.

III. RESULTS

Figure 4 shows the orientation-dependent ionization signal for different field configurations acting on the ground state HeH$^+$, shown in Fig. 1, at a Keldysh parameter of $\gamma = 0.34$. All curves are normalized such that the maximum value is 1. We see three qualitatively different behaviors. First, the exact tunneling rate shows a symmetric signal becoming maximal at $180°$ (ionization via the H side) and minimal at $0°$ (via the He side) with a value of approximately 21% relative to the maximum. This behavior is very well reproduced by the ionization yield obtained with the two-color fields (CRTC and LPTC), which give a minimal value of about 20%. A slightly different behavior can be seen for the CP pulse. Here we use the SSS with one PMD obtained for $\vec{R} \parallel \hat{y}$. A comparison with the MSS for CP fields is shown later in Fig. 6. Because our mapping ignores Coulomb effects, we see a small shift of the curve towards smaller angles so that the maximum is found around $176°$. This rotation is known as the attoclock angle. The minimum at a value of approximately 23% is slightly
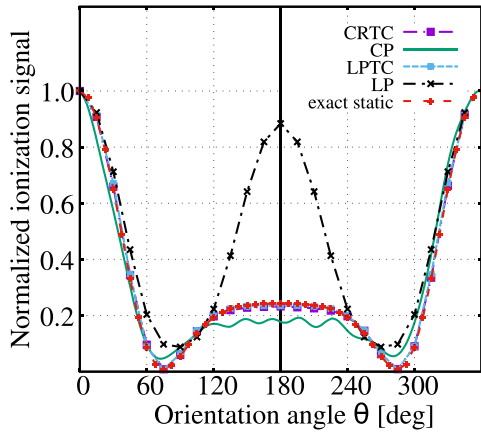
FIG. 5. Same as Fig. 4 but for the first excited state of HeH$^+$, a peak electric-field strength $E_{peak} \approx 0.0542$ a.u., and a fundamental wavelength of $\lambda = 3000$ nm.

too large. This is caused by a slightly smaller electric-field strength when the field is antiparallel to the molecular axis ($\theta = 180°$) compared to $\theta = 0$, due to the envelope of the pulse. Additionally, convolution of different orientations in the integration window or a small nonadiabatic effect may contribute. Finally, as expected, the LP pulse mixes two opposite orientations, which leads to a "wrong" behavior with an additional maximum at $0°$ and two minima at $90°$ and $270°$. This also causes a broadening of the main peak at $180°$. The difference in yield for $0°$ and $180°$ is approximately 6.5%, caused by the few-cycle nature of the pulse. Longer pulses lead to a more symmetric signal. Therefore, the pure LP pulses cannot be used to extract the orientation-dependent tunneling rate.

The ground state of HeH$^+$ exhibits no nodal lines. Previous work for O$_2$ [47] showed in the context of the strong-field approximation that nonadiabatic effects can modify the orientation-dependent ionization signal from a CP pulse substantially when nodal planes exist. Motivated by this, we repeat our simulations with the first excited state of the HeH$^+$ model, shown in Fig. 2. This state shows a nodal line at around $195°$ and $345°$ in the electron density, when the molecule is aligned with the y axis, $\vec{R} \parallel \hat{y}$. Aligning the negative electric field with one of the nodal lines is expected to result in a strong suppression of ionization. Considering that the first excited state of the HeH$^+$ ion is antibonding, we notice the limitations of the used fixed-nuclei approximation and we emphasize that the excited state of our model system should be viewed as a demonstration example of orbitals with nodal structure.

Figure 5 shows the results for the normalized orientation-dependent ionization signal for the first excited state of HeH$^+$. We adjust the maximal field strength in this calculation to the lower value $E_{peak} \approx 0.0542$ a.u. to avoid depletion of the state. Compared to the calculations for the ground state, a similar adiabaticity of $\gamma \approx 0.36$ is achieved by increasing the wavelength to $\lambda = 3000$ nm. The exact tunneling rate shows that the maximal ionization proceeds now over the He side ($\theta = 0°$), which is the opposite direction compared to the ground state. Further, we see two angles ($75°$ and $285°$) where

the ionization rate drops under 0.8%, which corresponds to ionization along the nodes of the state. A smaller second maximum is found at $180°$ at a value of 24%. The signal is symmetric.

The two-color fields (CRTC and LPTC) again reproduce the static rate very well up to an absolute difference of 1.2%. The LP pulse shows a similar behavior as for the ground-state calculation and mixes the two opposite angles leading to wrong results considering the height of the second maximum as well as the positions and values of the minima. The orientation-dependent ionization signal obtained after ionization with the CP pulse (SSS) reproduces roughly the trend of the exact tunneling rate, but additionally shows some significantly different features. First, we see an approximately periodic modulation on top of the maximum around $180°$. The modulation seems to be caused by interference of distinct contributions originating from different ionization times or pathways. Second, the signal around $180°$ is too small. This is caused by the envelope function of the CP pulse. By repeating the static simulation with a 4% smaller electric-field strength, we can reproduce the reduced averaged ionization signal at $180°$. In other words, the ratio between both maxima is sensitive to the instantaneous field strength and the field strength after a half cycle is already too small in an 11-cycle (110-fs) pulse to achieve a sufficiently constant electric-field strength for the central cycle. We have performed two additional simulations to support this idea. On the one hand, we have used a longer pulse with 15 cycles (150 fs). While the modulation is approximately unchanged, the ratio between the signal at $0°$ and $180°$ is in better agreement with the static tunneling rate. On the other hand, we have used a flat-top envelope function $f(t) \equiv 1$ with a smooth turn on and turn off within one cycle. In this way, we have several cycles of equal field strength in all directions. By varying the pulse length, we see that the modulation appears to vanish and the averaged signal at $180°$ slowly converges towards the exact tunneling rate. A third feature visible in Fig. 5 is a slight asymmetry. This is caused by two independent effects. The curve shows again a small attoclock angle towards smaller values. Hence, for orientation angles below $60°$ the yield is smaller than the exact tunneling rate and it is larger above $300°$. Further, the positions of both minima are shifted to smaller angles. In addition, nonadiabatic effects might lead to variations in the yield and an asymmetry. The left minimum exhibits a slightly smaller value than the right one. Nevertheless, a fourth and major drawback of the CP pulse is that both minima drop only to approximately 5%, not reaching the minimal value of the exact tunneling rate. This is similar to the observations in [47].

In Fig. 6 the comparison of the SSS and MSS for CP pulses is shown. In contrast to the SSS, the field strength at the time of ionization in the MSS is the same for all orientation angles. This leads to overall better agreement with the exact static result. For the ground state, the atto-clock shift is still present in the MSS, but the level of the minimum is now more accurate with an absolute difference of 0.3%. This is even better than the above results with CRTC and LPTC fields. We expect that optimizing the integration area in the MSS for CRTC fields might improve their accuracy too. For the excited state, the above-mentioned
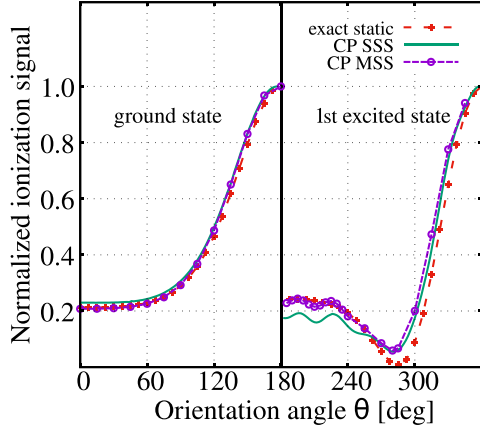
FIG. 6. Comparison of the normalized ionization signal obtained from TDSE solutions in the SSS and MSS for CP pules. For orientation angles below 180°, we show the ground-state results analogous to Fig. 4; for angles larger than 180°, we show the excited-state results analogous to Fig. 5.

FIG. 7. Normalized ionization signal obtained from TDSE solutions for the first excited state of HeH$^+$ for CP (SSS) and CRTC (MSS) fields at two wavelengths, compared to the exact tunneling rate. A peak electric-field strength $E_{\text{peak}} \approx 0.0542$ a.u. is used.

envelope effect is suppressed, but the modulation is still present. The positions and values of the minima due to the orbital nodal structure are similar to those obtained in the SSS.

To investigate the wavelength dependence of the modulation as well as the nonadiabatic effects, we repeat the computation with a fundamental wavelength of $\lambda = 2000$ nm, corresponding to a Keldysh parameter of $\gamma \approx 0.54$. Figure 7 shows the comparison of the orientation-dependent ionization signal of the CP (SSS) and CRTC (MSS) fields for 2000 and 3000 nm together with the exact tunneling rate. Whereas the signal of the CP pulse at 3000 nm roughly follows the exact rate, at 2000 nm a huge variation overlays the yield. We have confirmed that these modulations are also present in the MSS. When analyzing the individual PMDs of the MSS for different orientations, we noticed that the modulations are, by and large, rotated together with the molecule and that the contrast (ratio between maxima and minima) becomes maximal when $\vec{R} \parallel \hat{y}$. Neither the position of the maxima at 0° and 180° nor the two minima are clearly visible. Thus, the characteristics of the orbital nodal structure have entirely disappeared. The modulation around 180° is enhanced and extends towards all angles. Furthermore, the frequency of the modulation has changed. We have checked with intermediate wavelengths that the transition from 2000 nm to 3000 nm is smooth, thus excluding a resonance phenomenon. To extract from this orientation dependence any information about the ionized orbital would require a sophisticated modeling. However, adding a second color, which generates the CRTC field, the modulation is almost completely suppressed. The orientation-dependent ionization yield for the CRTC pulse at 2000 nm reproduces the static rate very well with a maximal absolute difference of 6.5% at 30°. The asymmetry becomes less pronounced at longer wavelengths, indicating a nonadiabatic effect. In none of the calculations does the total ionization yield exceed 0.1%, i.e., depletion is avoided.
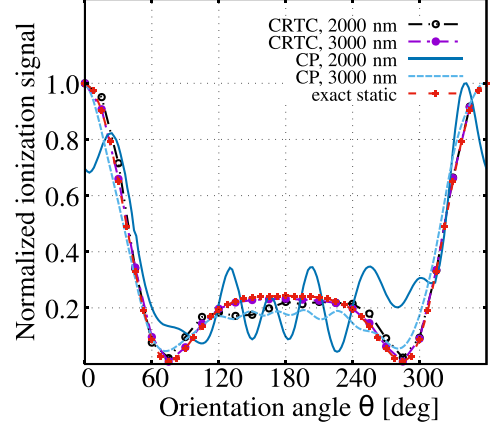
IV. CONCLUSION

We have shown that the orientation-dependent ionization yield obtained with linearly polarized single-color pulses cannot be used to measure the exact tunneling rate of an asymmetric molecule, because two opposite orientations are mixed. Circularly polarized pulses in the single-shot scheme, although convenient in experiments, are not ideal to measure the quasistatic limit either, in particular for an orbital with nodal structure, because even for quite long wavelengths, in none of our simulation are the node-induced minima reproduced well and interference effects complicate the signal. In addition, Coulomb effects complicate the analysis for circular polarization, as the direction of the ionizing electric field must be mapped to a final momentum. The effect of time-varying field strength during a short envelope can be eliminated by the multishot scheme, i.e., by measuring PMDs for many molecular orientations. We believe that these conclusions hold qualitatively also for more complex orbitals with nodal structure, such as π orbitals.

As an alternative to single-color circular polarization, we have shown that the orientation-dependent ionization yield using two-color fields is less disturbed by nonadiabatic effects and agrees better with the exact tunneling rate. While two-color linearly polarized pulses can be used to measure the orientation-dependent ionization yield, the counterrotating two-color (bicircular) field can be used to extract additionally the attoclock shift [55]. This observable can be measured independently, especially at wavelengths where circularly polarized fields are difficult to analyze.

Long pulses might also help suppress the envelope effects, at the cost of extending the timescale of ionization into the region where nuclear motion becomes relevant and where postionization alignment may play a role [72], which could pose a challenge to the analysis of experiments. We have restricted ourselves to relatively short laser pulses since our model operates under the limitations of the frozen-nuclei approximation. Future studies could explore how the benefits of two-color fields persist when averaging

over the width of nuclear wave packets. However, because many candidate molecules for such studies, such as the NO molecule [9,28], consist of nuclei much heavier than those of HeH^+, we believe that nuclear motion may often play a minor role.

[1] L. D. Landau and E. M. Lifshitz, *Quantum Mechanics: Non-Relativistic Theory*, 3rd ed. (Butterworth-Heinemann, Oxford, 1977).

[2] A. McPherson, G. Gibson, H. Jara, U. Johann, T. S. Luk, I. A. McIntyre, K. Boyer, and C. K. Rhodes, Studies of multiphoton production of vacuum-ultraviolet radiation in the rare gases, J. Opt. Soc. Am. B **4**, 595 (1987).

[3] T. Zuo, A. Bandrauk, and P. Corkum, Laser-induced electron diffraction: A new tool for probing ultrafast molecular dynamics, Chem. Phys. Lett. **259**, 313 (1996).

[4] M. Lein, J. P. Marangos, and P. L. Knight, Electron diffraction in above-threshold ionization of molecules, Phys. Rev. A **66**, 051404(R) (2002).

[5] M. Meckel, D. Comtois, D. Zeidler, A. Staudte, D. Pavičić, H. C. Bandulet, H. Pépin, J. C. Kieffer, R. Dörner, D. M. Villeneuve, and P. B. Corkum, Laser-induced electron tunneling and diffraction, Science **320**, 1478 (2008).

[6] C. I. Blaga, J. Xu, A. D. DiChiara, E. Sistrunk, K. Zhang, P. Agostini, T. A. Miller, L. F. DiMauro, and C. D. Lin, Imaging ultrafast molecular dynamics with laser-induced electron diffraction, Nature (London) **483**, 194 (2012).

[7] B. Belsa, K. M. Ziems, A. Sanchez, K. Chirvi, X. Liu, S. Gräfe, and J. Biegert, Laser-induced electron diffraction in the over-the-barrier-ionization regime, Phys. Rev. A **106**, 043105 (2022).

[8] Y. Huismans, A. Rouzée, A. Gijsbertsen, J. H. Jungmann, A. S. Smolkowska, P. S. W. M. Logman, F. Lépine, C. Cauchy, S. Zamith, T. Marchenko, J. M. Bakker, G. Berden, B. Redlich, A. F. G. van der Meer, H. G. Muller, W. Vermin, K. J. Schafer, M. Spanner, M. Y. Ivanov, O. Smirnova *et al.*, Time-resolved holography with photoelectrons, Science **331**, 61 (2011).

[9] S. G. Walt, N. Bhargava Ram, M. Atala, N. I. Shvetsov-Shilovski, A. von Conta, D. Baykusheva, M. Lein, and H. J. Wörner, Dynamics of valence-shell electrons and nuclei probed by strong-field holography and rescattering, Nat. Commun. **8**, 15651 (2017).

[10] C. Figueira de Morisson Faria and A. S. Maxwell, It is all about phases: Ultrafast holographic photoelectron imaging, Rep. Prog. Phys. **83**, 034401 (2020).

[11] T. Brabec, M. Côté, P. Boulanger, and L. Ramunno, Theory of tunnel ionization in complex systems, Phys. Rev. Lett. **95**, 073001 (2005).

[12] D. Pavičić, K. F. Lee, D. M. Rayner, P. B. Corkum, and D. M. Villeneuve, Direct measurement of the angular dependence of ionization for N_2, O_2, and CO_2 in intense laser fields, Phys. Rev. Lett. **98**, 243001 (2007).

[13] A. Staudte, S. Patchkovskii, D. Pavičić, H. Akagi, O. Smirnova, D. Zeidler, M. Meckel, D. M. Villeneuve, R. Dörner, M. Y. Ivanov, and P. B. Corkum, Angular tunneling ionization probability of fixed-in-space H_2 molecules in intense laser pulses, Phys. Rev. Lett. **102**, 033004 (2009).

[14] H. Akagi, T. Otobe, A. Staudte, A. Shiner, F. Turner, R. Dörner, D. M. Villeneuve, and P. B. Corkum, Laser tunnel ionization from multiple orbitals in HCl, Science **325**, 1364 (2009).

[15] D. Dimitrovski, C. P. J. Martiny, and L. B. Madsen, Strong-field ionization of polar molecules: Stark-shift-corrected strong-field approximation, Phys. Rev. A **82**, 053404 (2010).

[16] L. Holmegaard, J. L. Hansen, L. Kalhøj, S. L. Kragh, H. Stapelfeldt, F. Filsinger, J. Küpper, G. Meijer, D. Dimitrovski, M. Abu-samha, C. P. J. Martiny, and L. Bojer Madsen, Photoelectron angular distributions from strong-field ionization of oriented molecules, Nat. Phys. **6**, 428 (2010).

[17] D. Dimitrovski, M. Abu-samha, L. B. Madsen, F. Filsinger, G. Meijer, J. Küpper, L. Holmegaard, L. Kalhøj, J. H. Nielsen, and H. Stapelfeldt, Ionization of oriented carbonyl sulfide molecules by intense circularly polarized laser pulses, Phys. Rev. A **83**, 023405 (2011).

[18] H. Li, D. Ray, S. De, I. Znakovskaya, W. Cao, G. Laurent, Z. Wang, M. F. Kling, A. T. Le, and C. L. Cocke, Orientation dependence of the ionization of CO and NO in an intense femtosecond two-color laser field, Phys. Rev. A **84**, 043429 (2011).

[19] O. I. Tolstikhin, T. Morishita, and L. B. Madsen, Theory of tunneling ionization of molecules: Weak-field asymptotics including dipole effects, Phys. Rev. A **84**, 053423 (2011).

[20] J. Wu, L. P. H. Schmidt, M. Kunitski, M. Meckel, S. Voss, H. Sann, H. Kim, T. Jahnke, A. Czasch, and R. Dörner, Multiorbital tunneling ionization of the CO molecule, Phys. Rev. Lett. **108**, 183001 (2012).

[21] J. L. Hansen, L. Holmegaard, J. H. Nielsen, H. Stapelfeldt, D. Dimitrovski, and L. B. Madsen, Orientation-dependent ionization yields from strong-field ionization of fixed-in-space linear and asymmetric top molecules, J. Phys. B **45**, 015101 (2012).

[22] P. Krause and H. B. Schlegel, Angle-dependent ionization of small molecules by time-dependent configuration interaction and an absorbing potential, J. Phys. Chem. Lett. **6**, 2140 (2015).

[23] T. Endo, A. Matsuda, M. Fushitani, T. Yasuike, O. I. Tolstikhin, T. Morishita, and A. Hishikawa, Imaging electronic excitation of NO by ultrafast laser tunneling ionization, Phys. Rev. Lett. **116**, 163002 (2016).

[24] V.-H. Hoang, S.-F. Zhao, V.-H. Le, and A.-T. Le, Influence of permanent dipole and dynamic core-electron polarization on tunneling ionization of polar molecules, Phys. Rev. A **95**, 023407 (2017).

[25] F. Schell, T. Bredtmann, C. P. Schulz, S. Patchkovskii, M. J. J. Vrakking, and J. Mikosch, Molecular orbital imprint in laser-driven electron recollision, Sci. Adv. **4**, eaap8148 (2018).

[26] J. Yan, W. Xie, M. Li, K. Liu, S. Luo, C. Cao, K. Guo, W. Cao, P. Lan, Q. Zhang, Y. Zhou, and P. Lu, Photoelectron ionization time of aligned molecules clocked by attosecond angular streaking, Phys. Rev. A **102**, 013117 (2020).

[27] M. Abu-samha and L. B. Madsen, Multielectron effects in strong-field ionization of the oriented OCS molecule, Phys. Rev. A **102**, 063111 (2020).

[28] T. Endo, H. Fujise, H. Hasegawa, A. Matsuda, M. Fushitani, O. I. Tolstikhin, T. Morishita, and A. Hishikawa, Angle dependence of dissociative tunneling ionization of NO in asymmetric two-color intense laser fields, Phys. Rev. A **100**, 053422 (2019).

[29] I. S. Wahyutama, D. D. Jayasinghe, F. Mauger, K. Lopata, M. B. Gaarde, and K. J. Schafer, All-electron, density-functional-based method for angle-resolved tunneling ionization in the adiabatic regime, Phys. Rev. A **106**, 052211 (2022).

[30] A. M. Perelomov, V. S. Popov, and M. V. Terent'Ev, Ionization of atoms in an alternating electric field, Sov. Phys. JETP **23**, 924 (1966).

[31] A. M. Perelomov, V. S. Popov, and M. V. Terent'Ev, Ionization of atoms in an alternating electric field: II, Sov. Phys. JETP **24**, 207 (1967).

[32] M. V. Ammosov, N. B. Delone, and V. P. Krainov, Tunnel ionization of complex atoms and of atomic ions in an alternating electromagnetic field, Sov. Phys. JETP **64**, 1191 (1986).

[33] V. Kumarappan, L. Holmegaard, C. Martiny, C. B. Madsen, T. K. Kjeldsen, S. S. Viftrup, L. B. Madsen, and H. Stapelfeldt, Multiphoton electron angular distributions from laser-aligned CS_2 molecules, Phys. Rev. Lett. **100**, 093006 (2008).

[34] C. Z. Bisgaard, O. J. Clarkin, G. Wu, A. M. D. Lee, O. Geßner, C. C. Hayden, and A. Stolow, Time-resolved molecular frame dynamics of fixed-in-space CS_2 molecules, Science **323**, 1464 (2009).

[35] J. Ullrich, R. Moshammer, A. Dorn, R. Dörner, L. P. H. Schmidt, and H. Schmidt-Böcking, Recoil-ion and electron momentum spectroscopy: Reaction-microscopes, Rep. Prog. Phys. **66**, 1463 (2003).

[36] X. M. Tong, Z. X. Zhao, and C. D. Lin, Theory of molecular tunneling ionization, Phys. Rev. A **66**, 033402 (2002).

[37] A. Gazibegović-Busuladžić, D. Habibović, M. Busuladžić, and D. B. Milošević, Molecular strong-field approximation for photodetachment of electrons from homonuclear diatomic molecular anions, J. Opt. Soc. Am. B **37**, 813 (2020).

[38] D. Habibović, A. Gazibegović-Busuladžić, M. Busuladžić, A. Čerkić, and D. B. Milošević, Strong-field ionization of homonuclear diatomic molecules using orthogonally polarized two-color laser fields, Phys. Rev. A **102**, 023111 (2020).

[39] D. Habibović, A. Gazibegović-Busuladžić, M. Busuladžić, and D. B. Milošević, Strong-field ionization of heteronuclear diatomic molecules using an orthogonally polarized two-color laser field, Phys. Rev. A **103**, 053101 (2021).

[40] D. Habibović, A. Gazibegović-Busuladžić, M. Busuladžić, and D. B. Milošević, Characteristics of the molecular above-threshold ionization by a bichromatic elliptically polarized field with co-rotating components, J. Phys. B **55**, 085601 (2022).

[41] *Computational Strong-Field Quantum Dynamics*, edited by D. Bauer (de Gruyter, Berlin, 2017).

[42] T. K. Kjeldsen, C. Z. Bisgaard, L. B. Madsen, and H. Stapelfeldt, Influence of molecular symmetry on strong-field ionization: Studies on ethylene, benzene, fluorobenzene, and chlorofluorobenzene, Phys. Rev. A **71**, 013418 (2005).

[43] S. Petretti, Y. V. Vanne, A. Saenz, A. Castro, and P. Decleva, Alignment-dependent ionization of N_2, O_2, and CO_2 in intense laser fields, Phys. Rev. Lett. **104**, 223001 (2010).

[44] M. Abu-samha and L. B. Madsen, Multielectron effect in the strong-field ionization of aligned nonpolar molecules, Phys. Rev. A **106**, 013117 (2022).

[45] S.-K. Son and S.-I. Chu, Multielectron effects on the orientation dependence and photoelectron angular distribution of multiphoton ionization of CO_2 in strong laser fields, Phys. Rev. A **80**, 011403(R) (2009).

[46] G. G. Paulus, W. Nicklich, H. Xu, P. Lambropoulos, and H. Walther, Plateau in above threshold ionization spectra, Phys. Rev. Lett. **72**, 2851 (1994).

[47] I. Petersen, J. Henkel, and M. Lein, Signatures of molecular orbital structure in lateral electron momentum distributions from strong-field ionization, Phys. Rev. Lett. **114**, 103004 (2015).

[48] P. Eckle, M. Smolarski, P. Schlup, J. Biegert, A. Staudte, M. Schöffler, H. G. Muller, R. Dörner, and U. Keller, Attosecond angular streaking, Nat. Phys. **4**, 565 (2008).

[49] L. Torlina, F. Morales, J. Kaushal, I. Ivanov, A. Kheifets, A. Zielinski, A. Scrinzi, H. G. Muller, S. Sukiasyan, M. Ivanov, and O. Smirnova, Interpreting attoclock measurements of tunnelling times, Nat. Phys. **11**, 503 (2015).

[50] U. S. Sainadh, H. Xu, X. Wang, A. Atia-Tul-Noor, W. C. Wallace, N. Douguet, A. Bray, I. Ivanov, K. Bartschat, A. Kheifets *et al.*, Attosecond angular streaking and tunnelling time in atomic hydrogen, Nature (London) **568**, 75 (2019).

[51] D. Ray, F. He, S. De, W. Cao, H. Mashiko, P. Ranitovic, K. P. Singh, I. Znakovskaya, U. Thumm, G. G. Paulus, M. F. Kling, I. V. Litvinyuk, and C. L. Cocke, Ion-energy dependence of asymmetric dissociation of D_2 by a two-color laser field, Phys. Rev. Lett. **103**, 223201 (2009).

[52] L. V. Keldysh, Ionization in the field of a strong electromagnetic wave, Sov. Phys. JETP **20**, 1307 (1965).

[53] N. Eicke and M. Lein, Attoclock with counter-rotating bicircular laser fields, Phys. Rev. A **99**, 031402(R) (2019).

[54] N. Eicke, S. Brennecke, and M. Lein, Attosecond-scale streaking methods for strong-field ionization by tailored fields, Phys. Rev. Lett. **124**, 043202 (2020).

[55] P. Winter and M. Lein, Bicircular attoclock with molecules as a probe of strong-field Stark shifts and molecular properties, Phys. Rev. A **109**, L020801 (2024).

[56] H. Eichmann, A. Egbert, S. Nolte, C. Momma, B. Wellegehausen, W. Becker, S. Long, and J. K. McIver, Polarization-dependent high-order two-color mixing, Phys. Rev. A **51**, R3414 (1995).

[57] O. Kfir, P. Grychtol, E. Turgut, R. Knut, D. Zusin, D. Popmintchev, T. Popmintchev, H. Nembach, J. M. Shaw, A. Fleischer, H. Kapteyn, M. Murnane, and O. Cohen, Generation of bright phase-matched circularly-polarized extreme ultraviolet high harmonics, Nat. Photon. **9**, 99 (2015).

[58] D. B. Milošević and W. Becker, Improved strong-field approximation and quantum-orbit theory: Application to ionization by a bicircular laser field, Phys. Rev. A **93**, 063418 (2016).

[59] M. Abu-samha and L. B. Madsen, Probing atomic and molecular targets by intense bicircular counter-rotating laser fields, J. Phys. B **51**, 135401 (2018).

[60] D. Habibović, A. Čerkić, M. Busuladžić, A. Gazibegović-Busuladžić, S. Odžak, E. Hasović, and D. B. Milošević, Molecules in a bicircular strong laser field, Opt. Quantum Electron. **50**, 214 (2018).

[61] S. Brennecke, S. Eckart, and M. Lein, Attoclock with bicircular laser fields as a probe of velocity-dependent tunnel-exit positions, J. Phys. B **54**, 164001 (2021).

[62] M. Feit, J. Fleck, and A. Steiger, Solution of the Schrödinger equation by a spectral method, J. Comput. Phys. **47**, 412 (1982).

[63] R. Kosloff and H. Tal-Ezer, A direct relaxation method for calculating eigenfunctions and eigenvalues of the Schrödinger equation on a grid, Chem. Phys. Lett. **127**, 223 (1986).

[64] F. Oppermann, N. Eicke, and M. Lein, Real-time propagator eigenstates, J. Phys. B **55**, 19LT01 (2022).

[65] F. Oppermann, The HeH^+ isotopologues in intense asymmetric laser fields, Ph.D. thesis, Gottfried Willhelm Leibniz University Hannover, 2023.

[66] T. G. Winter, M. D. Duncan, and N. F. Lane, Exact eigenvalues, electronic wavefunctions and their derivatives with respect to the internuclear separation for the lowest 20 states of the HeH^{2+} molecule, J. Phys. B **10**, 285 (1977).

[67] K. Pachucki, Born-Oppenheimer potential for HeH^+, Phys. Rev. A **85**, 042511 (2012).

[68] T. A. Green, H. H. Michels, J. C. Browne, and M. M. Madsen, Configuration interaction studies of the HeH^+ molecular ion. I Singlet sigma states, J. Chem. Phys. **61**, 5186 (1974).

[69] M. Lein, E. K. U. Gross, and V. Engel, Intense-field double ionization of helium: Identifying the mechanism, Phys. Rev. Lett. **85**, 4707 (2000).

[70] P. Virtanen, R. Gommers, T. E. Oliphant, M. Haberland, T. Reddy, D. Cournapeau, E. Burovski, P. Peterson, W. Weckesser, J. Bright, S. J. van der Walt, M. Brett, J. Wilson, K. J. Millman, N. Mayorov, A. R. J. Nelson, E. Jones, R. Kern, E. Larson, C. J. Carey *et al.*, SciPy 1.0: Fundamental algorithms for scientific computing in Python, Nat. Methods **17**, 261 (2020).

[71] A. Khan, D. Trabert, S. Eckart, M. Kunitski, T. Jahnke, and R. Dörner, Orientation-dependent dissociative ionization of H_2 in strong elliptic laser fields: Modification of the release time through molecular orientation, Phys. Rev. A **101**, 023409 (2020).

[72] X. M. Tong, Z. X. Zhao, A. S. Alnaser, S. Voss, C. L. Cocke, and C. D. Lin, Post ionization alignment of the fragmentation of molecules in an ultrashort intense laser field, J. Phys. B **38**, 333 (2005).